Plasma-Enhanced Molecular Layer Deposition of Phosphane-ene Polymer Films

Justin T. Lomax,[†] Eden Goodwin,[‡] P. G. Gordon,[‡] Christine McGuiness,[∥], Floryan Decampo[∥]

Seán T. Barry,[*‡] *and Paul J. Ragogna*[*†]

† Department of Chemistry, University of Western Ontario, 1151 Richmond St, London, ON, Canada, N6A 3K7

‡ Department of Chemistry, Carleton University, 1125 Colonel By Drive, Ottawa, ON, Canada, K1S 5B6

∥ 4500 McGinnis Ferry Rd, Alpharetta, GA 30005, United States

KEYWORDS

Molecular layer deposition, Phosphorus, Plasma-enhanced, Hydrophosphination, Coatings, Thin film deposition, Quartz crystal microbalance

ABSTRACT

A vapour phase molecular layer deposition (MLD) process generating phosphorus-rich phosphane-ene polymer networks was adapted from known solution phase methods and successfully used in a commercial atomic layer deposition tool. By using plasma-enhanced MLD on Si/SiO_2 and Al_2O_3 substrates, film deposition was carried out with a commercially available primary phosphine, *i*$BuPH_2$, paired with a known volatile cyclic siloxane precursor, tetramethyltetravinylcyclotetrasiloxane (D_4^{Vinyl}). The deposition process used radicals generated by an Ar plasma source to facilitate P-H addition to vinyl functionalities on D_4^{Vinyl} which yielded a growth per cycle of 0.6 – 2.0 Å, generating 10-120 nm films as determined by AFM and SEM measurements. Characterization of the films were carried out using X-ray photoelectron spectroscopy and oxygen scavenging capabilities were studied using a quartz crystal microbalance, showing an uptake of oxygen by a 12 nm depth of a freshly deposited polymer film.

INTRODUCTION

Molecular layer deposition (MLD) is a type of atomic layer deposition (ALD), where organic thin films are deposited from the vapour phase through sequential, self-limiting reactions, generating thin films with high tunability, uniformity, and conformality.[1] MLD as a technique was first discovered by Yoshimura *et al.* in 1991 to prepare polyimides through a diamine (2,4-diaminonitrobenzene or 4,4'-diaminodiphenyl ether) with pyrometallic dianhydride,[2] and since its introduction, many compounds have been employed as precursors to generate thin films of

materials with thicknesses on the nanometer scale. Examples include amides, ureas, thioureas, azomethines, and ethylene terephthalates.[3–6] MLD is still in its infancy as compared to ALD, and therefore, relatively few elements other than C, N, O, and S have been incorporated in these thin films, leaving many paths open for investigation.[1]

Emerging technologies such as high-capacity batteries and flexible microelectronic devices can leverage MLD films to solve problems that are preventing their widespread use and commercialization. Through formation of ultrathin, resilient, and flexible polymer networks, MLD will be a primary driver going forward. The Ragogna group has developed a method to synthesize robust phosphorus polymer networks from the bulk phase using a thermal or photoinitiator that show excellent surface adhesion, barrier properties to O_2, optical transparency in the visible spectrum, and thermal stability up to 400 °C.[7–9] Phosphane-ene polymer networks propagate by the formation of a phosphinyl radical, which adds to a vinyl cross-linking agent to propagate the polymer growth.[7,10–12]

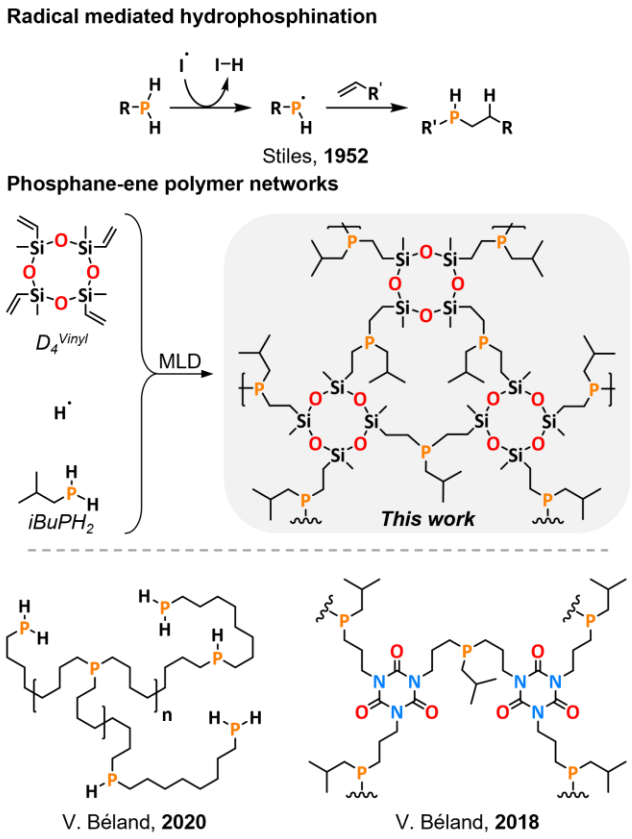

Figure 1. Generic radical-mediated hydrophosphination of alkene and phosphane-ene polymer networks.

These phosphane-ene polymer networks are a class of materials that can be easily tuned to bind transition metals and scavenge oxygen; it is this second characteristic that holds promise for these networks as packaging and protecting layers for flexible electronics. Phosphane-ene polymer networks are typically fabricated by reacting a primary phosphine (i.e., PH_3, $CyPH_2$, or iBuPH$_2$) and a multifunctional olefin crosslinking agent (Figure 1). By changing the composition of the monomer, the thermal, mechanical, and chemical properties of the resulting polymer can easily be

modified.[7,8,13] Since some typical vinyl crosslinkers showed reasonable volatility, it seemed viable to transfer this solution-phase polymerization chemistry to an MLD process (Figure 1a). In this context, we report successful MLD of a phosphane-ene polymer network, including careful thermal characterization of the deposition precursors isobutyl phosphine (*i*BuPH$_2$) and the vinyl crosslinker 2,4,6,8-tetramethyl-2,4,6,8-tetravinyl-cyclotetrasiloxane (D_4^{Vinyl}). To our knowledge this is the first documentation of radical mediated phosphine chemistry used in a molecular layer deposition process. These networks were tested for their reactivity with oxygen using a quartz crystal microbalance to monitor the mass gain of the deposited films in an oxygen-rich atmosphere.

RESULTS AND DISCUSSION

The volatility of D_4^{Vinyl} and *i*BuPH$_2$ were measured by thermogravimetric analysis (TGA) to determine the temperature of volatilization (T_V) and assess their viability as precursors. The T_V is defined as a temperature where the compound gives 1 Torr of vapor pressure. This definition arises from the expectation of what comprises a "good" vapor pressure from an industrial perspective: 1 Torr of vapor pressure supplies a significant flux of precursor in most industrial tools and is within the operating pressure of most ALD tools.

D_4^{Vinyl} exhibited a T_V of 52 °C with zero residual mass (Figure 2). The lack of residual mass demonstrates that there is no decomposition during evaporation, and along with the low T_V indicated an ideal vinyl crosslinker MLD precursor. The phosphine precursor *i*BuPH$_2$ was

extremely volatile and as a result, its T_V could not be accurately established. The *i*$BuPH_2$ volatilized at room temperature too quickly for a meaningful TGA trace to be obtained with respect to volatilization. Nevertheless, the TGA trace shows no residual mass, indicating *i*$BuPH_2$ is also a promising MLD precursor. During on-tool process development it was established that significant cooling (to 7 °C) was required to deliver a reasonable flux of *i*$BuPH_2$.

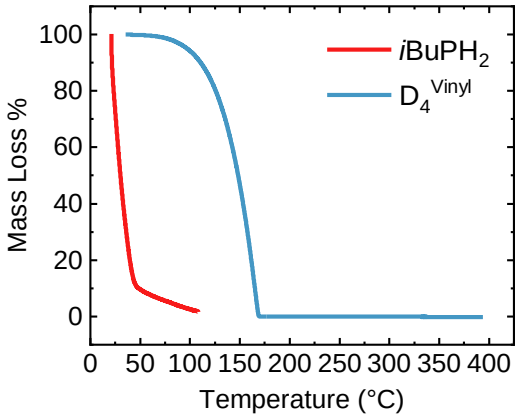

Figure 2. Thermal characterization of $^{i}BuPH_2$ and D_4^{Vinyl} by thermogravimetric analysis

A decomposition temperature as measured by differential scanning calorimetry (DSC) is also measured for vapor precursors to provide a "thermal range" between the temperature of volatilization and decomposition. However, D_4^{Vinyl} shows no decomposition between room temperature and 400 °C in a DSC experiment, with only an endotherm at 205 °C. This did not correspond to the melting point (-44 °C) or a known phase transition of the compound. A DSC for the $iBuPH_2$ could not be collected due to the extremely high volatility of the compound at low temperatures, which caused the sealed measurement pans to rupture before any relevant data could

be collected. These thermal characteristics suggested that the MLD should be a low-temperature process.

No film growth is observed with thermal MLD conditions using only *i*BuPH$_2$ and D$_4^{Vinyl}$ at 200°C. This was expected since the solution polymerization method requires a radical species for polymerization to be initiated.[7] A successful MLD process was developed using *i*BuPH$_2$, D$_4^{Vinyl}$ and an argon plasma ((Ar*)(5.0 Ar at 2800 W)), with the plasma serving as the radical mediator. A typical deposition began by heating the deposition chamber to 200 °C, followed by ten pulses of hydrogen plasma (5% H$_2$/Ar) to remove any surface contamination and to ensure that each of the depositions began with a standard, clean surface. The *i*BuPH$_2$ bubbler is cooled with a chiller to 7 °C and the D$_4^{Vinyl}$ precursor is held at 75 °C. The pulse program after the plasma clean consisted of a 0.1 s pulse of *i*BuPH$_2$ followed by a 10 s purge (N$_2$); a 0.1 s pulse of D$_4^{Vinyl}$ followed by a second 10 s purge; and a 10 s pulse of Ar plasma at 2800 W with no purge. These three pulses constituted a single cycle and typically 300 cycles are used to generate the films reported here.

We speculate that the *i*BuPH$_2$ precursor reacts with Ar* by the abstraction of a hydrogen from the *i*BuPH$_2$ to generate a phosphinyl radical to add to a surface vinyl functional group (Figure 3a). This leaves a second P-H bond remaining on the surface, and subsequent radical P$^\bullet$ formation will then add to the vinyl crosslinker D$_4^{Vinyl}$ when it is introduced into the chamber, propagating film growth.

In an attempt to promote substrate-enhanced growth during the MLD process, Al_2O_3 substrates are primed with a variety of carboxylic acids by dip-coating: acrylic acid (**AA**), pentanoic acid (**PA**), and undecylenic acid (**UA**) were each assessed as surface primers.[14] These primers are chosen to probe the effects of varying alkyl chain length of the vinyl functional group on phosphine nucleation. It is expected that, by providing initial surface-bound vinyl groups, the surface reactivity of the *i*BuPH• radical would be enhanced and promote film growth (Figure 3b).

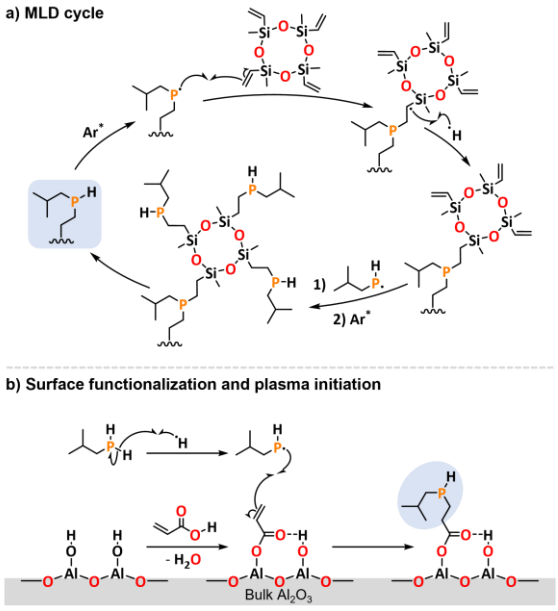

Figure 3. Proposed scheme of phosphane-ene film growth by MLD with *i*BuPH$_2$ and D_4^{Vinyl} mediated by an Ar plasma (Ar*) for radical initiation and propagation of precursors.

The saturation curve for the D_4^{Vinyl} precursor in the absence of a surface primer group (Figure 4) suggests saturated growth but with a higher than usual variability than expected for MLD processes. There may be competing reversible and irreversible surface nucleation that is causing

this variability, and further surface mechanistic studies will be required to determine how chemisorption and growth proceed in this process. A saturation curve for the *i*BuPH$_2$ is not shown as the ALD tool was unable to execute short enough pulses to examine sub-saturative growth, and the growth per cycle was 0.7 Å at all pulse lengths of *i*BuPH$_2$.

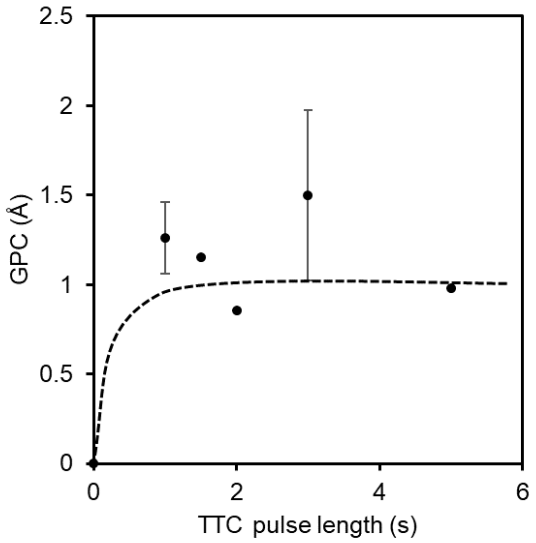

Figure 4. The saturation curve for D_4^{Vinyl}, with the *i*BuPH$_2$ pulse held at 0.1 s and indicated self-limiting behaviour.

Phosphane-ene films are analyzed through atomic force microscopy (AFM) to determine their thickness and surface morphology (Figure 5(i) and 5(ii)). Step-edges are created using Kapton tape to mask part of the substrate, and post-deposition, the tape was removed, with tape residue cleaned with isopropyl alcohol. 300-cycle depositions resulted in an average growth per cycle (GPC) of 0.7 Å. In addition to the characterization of the film thickness by AFM, focused ion beam scanning electron microscope (FIB-SEM) images were collected (Figure 5(iii)). The cross-section view of

the film was in good agreement with the thickness measured by AFM and showed the excellent conformality of the film deposited on SiO_2 with a film thickness of 20 nm after 300 cycles. The resulting films had a root-mean-squared (RMS) roughness of 4.7 Å, close to that measured for the substrate (9.0 Å). As is typical with MLD processes, the films had consistent and smooth coverage.[15,16]

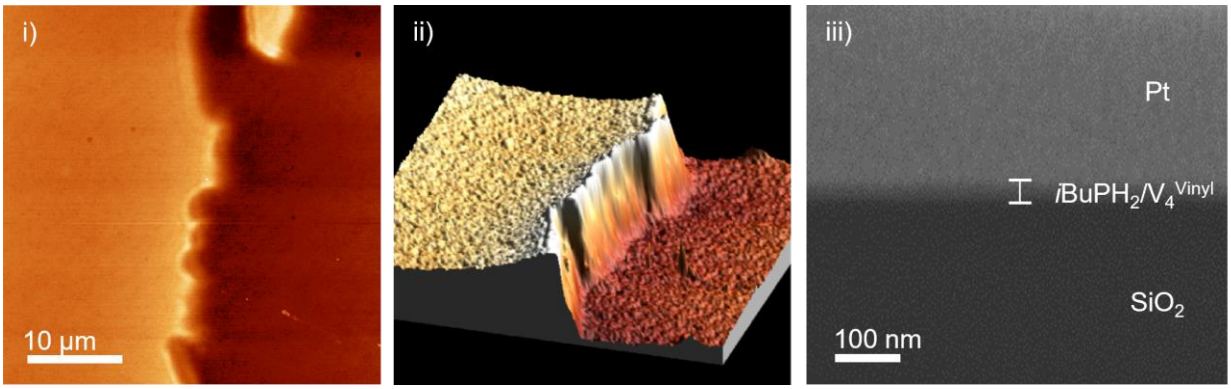

Figure 5. (i) AFM image of a phosphane-ene film with a step-edge of 90nm on a Si substrate. (ii) 3-D topographical AFM image of the film. (iii) FIB-SEM cross section of phosphane-ene film with a film thickness of 20 nm (contrast +100%).

Elemental composition and bonding environments of phosphane-ene films on Al_2O_3 were analyzed using X-ray photoelectron spectroscopy (XPS). To estimate the relative inclusion of both precursors (*i*$BuPH_2$ and D_4^{Vinyl}) in the film, a ratio of Si 2p and P 2p peak areas is calculated from XPS survey scans. Initial deposition trials were attempted with *i*$BuPH_2$ (0.1s pulse, 10s purge) and D_4^{Vinyl} (1s pulse, 10s purge) on **AA-**primed Al_2O_3 (**AA-**Al_2O_3). These films had 1.2% and 4.4% for Si 2p and P 2p, respectively, giving a ratio of 0.27:1 compared to an ideal ratio of 2:1, Si:P.

This lower ratio suggests incomplete reaction of D_4^{Vinyl}. This deposition was repeated with a pre-clean of 5% H_2/Ar plasma prior to primer adsorption, which improved the Si:P ratio to 0.44:1. XPS data from a similar run but using a longer D_4^{Vinyl} pulse (10s) gave a Si:P of 1.44:1, showing that longer D_4^{Vinyl} pulses increase the overall Si abundance in the film.

Although other primers were used in an attempt to promote substrate enhanced growth, all XPS data indicated that, in each case, the priming agents resulted in inferior films when compared to the bare substrates (Table 1). The literature provides a rationale for the observed film growth on bare Al_2O_3 substrates, where D_4^{Vinyl} can undergo ring opening on the Al_2O_3 surface, thus enabling film growth via the remaining, pendant vinyl functional groups.[17,18]

Table 1. Tabulated XPS data of P and Si atomic % from phosphane-ene MLD runs. Pulse parameters used were (i) *i*BuPH$_2$ (0.1s/10s), D_4^{Vinyl} (1s/10s), Ar$^{\bullet}$ (12s, 2800 W) with no H$^{\bullet}$ plasma clean, (ii) repeat of (i) with plasma clean, and (iii) repeat of (ii) with a 10 s D_4^{Vinyl} pulse. Each run consisted of 300 cycles.

		Si/P (Ratio of At%)		
Substrate	**Primer**	**i)**	**ii)**	**iii)**
Al_2O_3	**-**	0.59	0.67	2.19
	AA	0.27	0.44	1.44
	PA	0.28	0.09	1.83
	UA	0.24	0.42	1.49
Au	**-**	0.25	0.12	1.92
	AA	0.33	0	1.4
	PA	0.23	1.06	1.54
	UA	0	0	1.13

From XPS data, P 2p, Si 2p, and C 1s core-level spectra with peak-fitting are all modelled with Gaussian–Lorentzian (GL) functions and a Sherley background subtraction (Figure 6a). The P 2p spectra is deconvoluted into P(V) and P(III) states. For P(V), there was a signal for fully oxygen-bonded as well as oxygen and alkyl bonded phosphorus at 134.1 and 133.5 eV, respectively. This film also showed contributions from a fully alkyl bonded P(III) center at 130.7 eV. The abundance of P-O centers in the P 2p spectrum is attributed to surface oxidation from the ex-situ XPS analysis while PR_3 species for the film is a manifestation of P(III) bonding environments within the film that have not been oxidized as diffusion of O_2 had not reached the full depth of the film. The Si 2p spectrum displays one assignment of siloxane from the D_4^{Vinyl} at a binding energy (BE) of 102.6

eV.[19] Deconvolution of the C 1s spectra of the film on the Al_2O_3 substrate contains bonding configurations of C-Si-C and C-P=O with a BE of 284.3 and 286.8 eV, respectively.[20] The C 1s spectrum also showed some surface contaminants C-O-C, C=O, and O-C=O with BEs of 286.6, 287.8 and 289.0 eV, respectively and is attributed to adventitious carbon.[21,22] Given the inaccuracies that arise from adventitious carbon species, the area of the C-P=O connection in the C1s is higher than expected but overlaps with C-O-C binding energies which is a common impurity.

On the Au substrate, the C 1s window shows a lack of C-Si-C fittings which would be present for the D_4^{Vinyl} precursor. The P 2p XPS windows on Au substrates show P-Oxide content at higher binding energy. The negligible amount of Si suggests only residual (and potentially adventitiously oxidized) *i*$BuPH_2$ on the Au substrate.

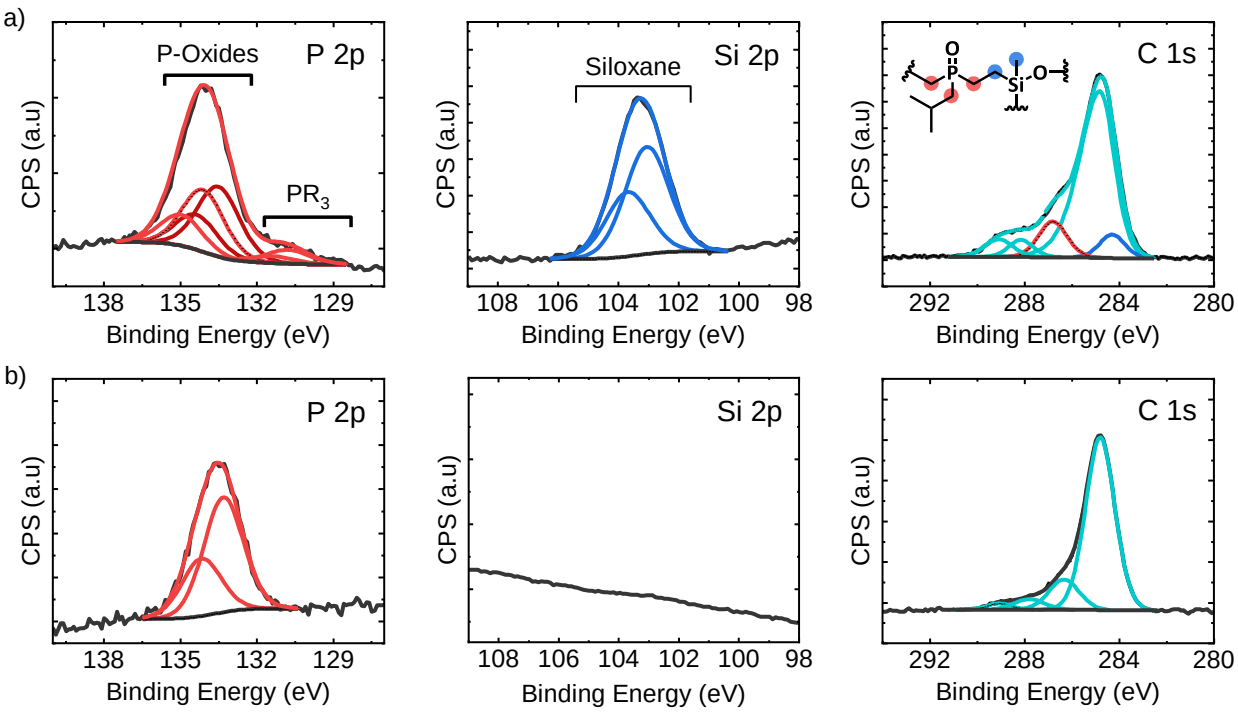

Figure 6. High-resolution P 2p, Si 2p and C 1s XPS spectra of films on a) Al_2O_3, At% (P 2p – 3.6%, Si 2p – 3.8%, C 1s – 22.2%) and b) Au, At% (P 2p – 8.7%, Si 2p – 0%, C 1s – 30.8%).

XPS depth profiling the deposited phosphane-ene film on Al_2O_3 yields interesting data pertaining to phosphorus oxidation (Figure 7a). When sputtered, the P 2p high resolution spectra are observed to change to a lower BE closer to the substrate (Δ -1.1eV). This is likely due to the phosphorus in the polymer reacting with atmospheric oxygen, whereas the deeper phosphorus sites are kinetically protected from reacting with O_2 by slow diffusion. This demonstrates the effective oxygen-getting character of the phosphane-ene film, illustrating its utility as a flexible electronic packaging film to prevent oxygen from accessing protected sublayers.

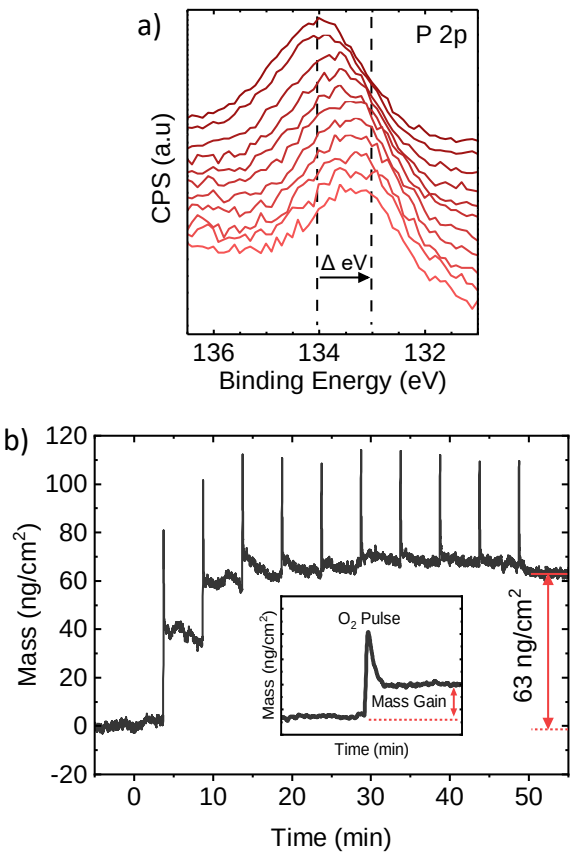

Figure 7. a) Stacked XPS High-resolution spectra of sputtered P 2p region indicating a shift from P^{V} to P^{III} species (Δ -1.1eV) b) Oxygen uptake QCM data for a phosphane-ene MLD film with an inset of mass gain from a single dry air pulse.

Quartz crystal microbalance (QCM) measurements is used to monitor the overall uptake of oxygen in a 48 nm MLD phosphane-ene film. Dry air (ten 0.1 s pulses with 5 min purges) was delivered to a freshly prepared polymer film deposited on an Al_2O_3-coated QCM crystal. Changes in areal mass density is monitored to determine the overall oxidation of the P sites. The QCM data shows an initial sharp pressure spikes coincident with the dry air pulses, with an increasing residual

mass following each pulse (Figure 7b; a selected pulse is shown in the inlay). After three pulses of dry air, a cumulative mass gain of 63 ng/cm^2 was achieved, suggesting that the oxygen load of the phosphane-ene film had been reached. This mass change equates to an uptake of 24 O atoms/nm^2. Assuming a 1:1 P:O uptake in the film this equates to a penetration depth of oxygen of 12 nm.

Conclusions

Phosphane-ene polymer network synthesis was effectively adapted from a solution-based method to gas phase MLD. In the proposed mechanism of film growth, the plasma-enhanced MLD process leveraged phosphinyl radical chemistry to add these species to C=C groups on a siloxane crosslinking agent (D_4^{Vinyl}) with GPCs of 0.6 – 2.0 Å and film thicknesses of 20 – 120 nm. XPS analysis highlighted bonding arrangements of P(III) and P(V) sites, demonstrating uptake of oxygen during incidental atmospheric exposure. To assess the O_2 scavenging ability of the film, a sputtered XPS depth profile was collected. A shift from P^V to P^{III} with increasing depth was observed, which indicated surface reactivity that slows diffusion of dioxygen through the film. Dioxygen uptake experiments by QCM characterization of unexposed, freshly prepared films showed a self-limiting mass gain of 63 ng/cm^2 equating to a penetration depth of 12 nm by oxygen of the polymer film. The high phosphorus loading and tunability of the phosphane-ene film demonstrates the promise as an oxygen scavenging packaging material, and the ability to deposit the film in a low temperature MLD process is compatible with flexible electronics manufacturing.

Experimental

Molecular Layer Deposition (MLD) Methods

All depositions were performed on a Picosun R-200 Advanced Plasma-Enhanced Atomic Layer Deposition (PE-ALD) tool. The substrates were mechanical grade silicon (100) or Al_2O_3-coated silicon (100). The substrates were kept in the cleanroom under ambient conditions until the wafers were diced into rectangular coupons approximately 1 cm x 3 cm for use. Gold substrates were produced by coating the mechanical grade Si wafers with approximately 100 nm of gold using a physical vapor deposition tool (Angstrom COVAP).

$^{i}BuPH_2$ and D_4^{Vinyl} were obtained from Solvay and Sigma Aldrich, respectively and used as received. The D_4^{Vinyl} was observed to become viscous over time in the heated bubbler (possibly as a result of precursor oligomerization) and so for each run the bubbler was only loaded with the amount necessary for that experiment. The $^{i}BuPH_2$ bubbler was filled with enough material for multiple runs as it showed no sign of decomposition. Each process began with a flush step repeated three times, where high purity (4.8 grade, 99.998%) nitrogen gas was used to fill the chamber to a pressure of 100 Torr, then evacuated to a base pressure of 5 Torr. The deposition chamber temperature was set to 200 °C and held at that temperature for 20 min prior to the precursor pulse sequence. The $^{i}BuPH_2$ bubbler was held in a chiller at 7 °C to lower its volatility (at room temperature a 0.1 s pulse delivered an enormous, wasteful excess of material on the order of 5 g). D_4^{Vinyl} was held at 75 °C in a "PicoSolid" bubbler and the lines above the bubbler were held at 80

°C to prevent condensation during transit. Process nitrogen flows were set as follows: $^{i}BuPH_2$ at 150 sccm, D_4^{Vinyl} and unused lines at 80 sccm, intermediate space (IMS) at 400 sccm. Plasma gas flows were as follows: 80 sccm carrier gas and 185 sccm plasma gas. The Ar* pulse consisted of a 0.4 s flow stabilization time, a 9 s plasma pulse (600 W) and no purge. The D_4^{Vinyl} pulse consisted of a 0.1 – 10 s pulse and a 10 s purge.

Atomic Force Microscopy (AFM) Measurements

Kapton tape was placed on the substrate prior to deposition to provide a step edge of the MLD film for AFM analysis. After deposition, the tape was removed, exposing the bare Si substrate below and cleaned with isopropyl alcohol and Kimwipes. AFM analysis was performed with a Dimension 3100 SPM/AFM over a ~50μm^2 analysis area.

X-ray Photoelectron Spectroscopy (XPS) Measurements

Samples were transferred without an air-break into a N_2 glovebox and sealed in airtight packaging to limit oxidation of the films prior to analysis. XPS analyses were carried out at Surface Science Western (SSW) with a Kratos AXIS Supra X-ray photoelectron spectrometer using a monochromatic Al Kα source (15mA, 15kV). Sample to a depth of 7 - 10 nanometres and has detection limits ranging from 0.1 - 0.5 atomic percent. The instrument work function was calibrated to give a binding energy (BE) of 285 eV for the C 1s. The Kratos charge neutralizer system was used on all specimens. Both the survey scan and high-resolution analyses were collected at a take-off angle of 90° with an analysis area of 300 x 700 microns and a pass energy

of 15 eV. CasaXPS (ver. 2.3.23) software was used for all deconvolution of spectra with a Shirley background subtraction. Spectra interpretation and fittings were done with fitting parameters and constraints collected from NIST. Depth profile experiments used an Ar cluster gun with a 5 KeV accelerating voltage and 2000 Ar atoms.

Scanning Electron Microscopy (SEM) Measurements

Leo Zeiss 1530 field emission FIB/SEM at Western's Nanofabrication facility with a magnification of 50,000x and an accelerating voltage of 3 kV. Cross-sections of prepared films on SiO_2 substrates were milled out with Mo ions and observed at an angle.

Quartz Crystal Microbalance (QCM) Measurements

All QCM measurements were conducted in a home-built hot walled tube furnace reactor on an in-situ quartz crystal microbalance (QCM, Colnatec, EON-LT) with a built-in temperature reader. Fresh QCM crystals (6MHz, AT-cut, Al_2O_3 electrodes) were coated and packaged as described above. The QCM was then assembled and installed into the reactor under air-free conditions. After assembly, the reactor was brought to process temperature (50 ^oC) and left to equilibrate under no flow (0 sccm) conditions for 24 hours.

After stabilizing, the polymer coated QCM crystal was intermittently exposed to 10 pulses (100ms) of dry air with 5-minute-long purges between pulses.

Adsorbed ar6eal mass density is derived from the Sauerbry equation[23]:

$$\frac{\Delta m}{A} = C\Delta F$$

Where the conversion factor C is:

$$C = -\frac{\sqrt{\rho\mu}}{2f_0^2}$$

Where density of a quartz crystal (ρ_q) is 2.648 g cm^{-3}, the shear modulus of an AT-cut crystal (μAT) is $2.947*10^{11}$g cm^{-1} s^{-2} and a resonant frequency of 6 MHz provides a conversion factor of -12.27 ng cm^{-2} Hz^{-1}

Areal oxygen density ($\#_O/A$) is calculated using the following relationship:

$$\frac{\#_O}{A} = \frac{N_A * (\Delta m/A)}{MW_o}$$

Where N_A is Avogadro's number, $\boldsymbol{\Delta m/A}$ is the areal mass density and MW_O is the molecular weight of oxygen.

Thermogravimetric Analysis

Air-free TGA was performed on a TA Instruments Discovery TGA 55 instrument housed in a nitrogen-filled (99.998%) MBraun Labmaster 130 glovebox. In a typical experiment approximately 25 mg of analyte was placed in a platinum pan and heated to 400 ºC with a ramp rate of 10 ºC/min. Nitrogen (99.999% purity, 60 sccm) was used as the process gas. Platinum pans were cleaned by sequential sonication in glacial acetic acid then isopropanol, followed by heating until red-hot with a propane torch.

Differential Scanning Calorimetry.

DSC experiments were performed with a TA Instruments Q10 instrument. The DSC was calibrated at the melting point of indium metal (156.6 ºC). All DSC samples were hermetically sealed in aluminum pans inside a glovebox prior to analysis. All samples were heated to 500 ºC with a ramp rate of 10 ºC/min, using nitrogen (99.998% purity, 50 sccm) as the process gas.

Author Information

Corresponding Author

Paul J. Ragogna,

Western University, London, ON, N6A 5B7, Canada

Email: pragogna@uwo.ca

Notes

The authors declare no competing financial interest.

Author Contributions

The manuscript was written through contributions of all authors. All authors have given approval to the final version of the manuscript.

Funding Sources

The Natural Sciences and Engineering Research Council of Canada (NSERC), Solvay Canada, Ontario Ministry of Research and Innovation (OMRI), and Canadian Foundations for Innovation (CFI).

ACKNOWLEDGMENTS

The authors would like to thank, the Natural Sciences and Engineering Council of Canada (NSERC), the Canada Foundation for Innovation (CFI), Solvay Specialty Polymers, Surface Science Western (SSW; Drs. M. Biesinger and J. Henderson), the Western Nanofabrication Facility, Carleton Nanofab, Western University and Carleton University for their support.

REFERENCES

(1) Meng, X. An Overview of Molecular Layer Deposition for Organic and Organic–Inorganic Hybrid Materials: Mechanisms, Growth Characteristics, and Promising Applications. *J. Mater. Chem. A* **2017**, *5* (35), 18326–18378. https://doi.org/10.1039/C7TA04449F.

(2) Yoshimura, T.; Tatsuura, S.; Sotoyama, W. Polymer Films Formed with Monolayer Growth Steps by Molecular Layer Deposition. *Appl. Phys. Lett.* **1991**, *59* (4), 482–484. https://doi.org/10.1063/1.105415.

(3) Kim, A.; Filler, M. A.; Kim, S.; Bent, S. F. Layer-by-Layer Growth on Ge(100) via Spontaneous Urea Coupling Reactions. *J. Am. Chem. Soc.* **2005**, *127* (16), 6123–6132. https://doi.org/10.1021/ja042751x.

(4) Yoshimura, T.; Tatsuura, S.; Sotoyama, W.; Matsuura, A.; Hayano, T. Quantum Wire and Dot Formation by Chemical Vapor Deposition and Molecular Layer Deposition of One-dimensional Conjugated Polymer. *Appl. Phys. Lett.* **1992**, *60* (3), 268–270. https://doi.org/10.1063/1.106681.

(5) Ivanova, T. V.; Maydannik, P. S.; Cameron, D. C. Molecular Layer Deposition of Polyethylene Terephthalate Thin Films. *Journal of Vacuum Science & Technology A* **2012**, *30* (1), 01A121. https://doi.org/10.1116/1.3662846.

(6) Loscutoff, P. W.; Lee, H.-B.-R.; Bent, S. F. Deposition of Ultrathin Polythiourea Films by Molecular Layer Deposition. *Chem. Mater.* **2010**, *22* (19), 5563–5569. https://doi.org/10.1021/cm1016239.

(7) Guterman, R.; Rabiee Kenaree, A.; Gilroy, J. B.; Gillies, E. R.; Ragogna, P. J. Polymer Network Formation Using the Phosphane–Ene Reaction: A Thiol–Ene Analogue with Diverse Postpolymerization Chemistry. *Chem. Mater.* **2015**, *27* (4), 1412–1419. https://doi.org/10.1021/cm504784e.

(8) Béland, V. A.; Ragogna, P. J. Metallized Phosphane–Ene Polymer Networks as Precursors for Ceramics with Excellent Shape Retention. *ACS Appl. Mater. Interfaces* **2020**, *12* (24), 27640–27650. https://doi.org/10.1021/acsami.0c09044.

(9) Cuthbert, T. J.; Guterman, R.; Gillies, E. R.; Blacquiere, J.; Gilroy, J.; Ragogna, P. J. Polymerization of Primary Phosphines with Olefins to Generate Phosphorus Based Polymer Networks. US20200270399A1, August 27, 2020.

(10) Béland, V. A.; Wang, Z.; Sham, T.-K.; Ragogna, P. J. Antimony-Functionalized Phosphine-Based Photopolymer Networks. *Angewandte Chemie International Edition* **2018**, *57* (40), 13252–13256. https://doi.org/10.1002/anie.201806235.

(11) Béland, V. A.; Ragogna, P. J. Metallized Phosphane–Ene Polymer Networks as Precursors for Ceramics with Excellent Shape Retention. *ACS Appl. Mater. Interfaces* **2020**, *12* (24), 27640–27650. https://doi.org/10.1021/acsami.0c09044.

(12) Stiles, A. R.; Rust, F. F.; Vaughan, W. E. The Preparation of Organo-Phosphines by the Addition of Phosphine to Unsaturated Compounds. *J. Am. Chem. Soc.* **1952**, *74* (13), 3282–3284. https://doi.org/10.1021/ja01133a018.

(13) Béland, V. A.; Wang, Z.; Sham, T.-K.; Ragogna, P. J. Polymer Networks Functionalized with Low-Valent Phosphorus Cations. *Journal of Polymer Science n/a* (n/a). https://doi.org/10.1002/pol.20220227.

(14) Lin, S.-Y.; Tsai, T.-K.; Lin, C.-M.; Chen, C.; Chan, Y.-C.; Chen, H.-W. Structures of Self-Assembled Monolayers of n-Alkanoic Acids on Gold Surfaces Modified by Underpotential

Deposition of Silver and Copper: Odd−Even Effect. *Langmuir* **2002**, *18* (14), 5473–5478. https://doi.org/10.1021/la0157364.

(15) Barranco, V.; Carpentier, J.; Grundmeier, G. Correlation of Morphology and Barrier Properties of Thin Microwave Plasma Polymer Films on Metal Substrate. *Electrochimica Acta* **2004**, *49* (12), 1999–2013. https://doi.org/10.1016/j.electacta.2003.12.030.

(16) Coclite, A. M.; Howden, R. M.; Borrelli, D. C.; Petruczok, C. D.; Yang, R.; Yagüe, J. L.; Ugur, A.; Chen, N.; Lee, S.; Jo, W. J.; Liu, A.; Wang, X.; Gleason, K. K. 25th Anniversary Article: CVD Polymers: A New Paradigm for Surface Modifi Cation and Device Fabrication. *Advanced Materials* **2013**, *25* (38), 5392–5423. https://doi.org/10.1002/adma.201301878.

(17) Jones, R. G.; Ando, W.; Chojnowski, J. *Silicon-Containing Polymers: The Science and Technology of Their Synthesis and Applications*; Springer Science & Business Media, 2013.

(18) Ashurbekova, K.; Ashurbekova, K.; Saric, I.; Gobbi, M.; Modin, E.; Chuvilin, A.; Petravic, M.; Abdulagatov, I.; Knez, M. Ultrathin Hybrid SiAlCOH Dielectric Films through Ring-Opening Molecular Layer Deposition of Cyclic Tetrasiloxane. *Chem. Mater.* **2021**, *33* (3), 1022–1030. https://doi.org/10.1021/acs.chemmater.0c04408.

(19) O'Hare, L.-A.; Parbhoo, B.; Leadley, S. R. Development of a Methodology for XPS Curve-Fitting of the Si 2p Core Level of Siloxane Materials. *Surface and Interface Analysis* **2004**, *36* (10), 1427–1434. https://doi.org/10.1002/sia.1917.

(20) O'Hare, L.-A.; Hynes, A.; Alexander, M. R. A Methodology for Curve-Fitting of the XPS Si 2p Core Level from Thin Siloxane Coatings. *Surface and Interface Analysis* **2007**, *39* (12–13), 926–936. https://doi.org/10.1002/sia.2634.

(21) Barr, T. L.; Seal, S. Nature of the Use of Adventitious Carbon as a Binding Energy Standard. *Journal of Vacuum Science & Technology A: Vacuum, Surfaces, and Films* **1995**, *13* (3), 1239–1246. https://doi.org/10.1116/1.579868.

(22) Swift, P. Adventitious Carbon—the Panacea for Energy Referencing? *Surface and Interface Analysis* **1982**, *4* (2), 47–51. https://doi.org/10.1002/sia.740040204.

(23) Johannsmann, D. *The Quartz Crystal Microbalance in Soft Matter Research*; Soft and Biological Matter; Springer International Publishing: Cham, 2015. https://doi.org/10.1007/978-3-319-07836-6.